Earth and Planetary Science Letters 406 (2014) 165–173

Contents lists available at ScienceDirect

Earth and Planetary Science Letters

www.elsevier.com/locate/epsl

Pressure-induced elastic and structural changes in hydrous basalt glasses: The effect of H_2O on the gravitational stability of basalt melts at the base of the upper mantle

Lei Wu [a], De-Bin Yang [a], Hong-Sen Xie [b], Fang-Fei Li [a], Bo Hu [a], Yang Yu [a], Wen-Liang Xu [a], Chun-Xiao Gao [a,*]

[a] State Key Laboratory of Superhard Materials, College of Earth Sciences, Jilin University, Changchun 130012, China
[b] Laboratory of the Earth's Interior and Geofluid Geochemistry, Institute of Geochemistry, Chinese Academy of Sciences, Guiyang 550002, China

ARTICLE INFO

Article history:
Received 1 April 2014
Received in revised form 26 August 2014
Accepted 2 September 2014
Available online 30 September 2014
Editor: J. Brodholt

Keywords:
Brillouin scattering
hydrous basalt glass
sound velocities
compressibility
depolymerization

ABSTRACT

To understand the effect of hydration on the elastic properties of silicate melts, we conducted in situ high-pressure Brillouin scattering measurements on two hydrous basalt glasses with different water contents in diamond anvil cells. Second-order phase transitions were observed in the hydrous basalt glasses and are due to the topological rearrangement of the silicate network to a high [Si, Al]–O coordination. Up to a pressure of 10 GPa at 300 K, the extra 2.23 wt% H_2O lowers the elastic moduli of FX-2 basalt glass (2.69 wt% H_2O) by 10%–18%, but does not affect the pressure derivatives of the elastic moduli, compared with FX-1 (0.46 wt% H_2O) basalt glass. The phase transition takes place at a higher pressure in FX-2 compared with FX-1, possibly because of the depolymerization of water to silicate glass. Water interacts with network-forming cations and creates Si–OH and Al–OH groups, and prohibits nonbridging oxygen ions from being connected to other nearby framework cations (i.e., $^{[5,6]}$(Si, Al)), resulting in the hysteresis of the second-order phase transition. The density contrasts of our hydrous basalt melts with previous mid-ocean ridge basalt and preliminary reference Earth model data indicate that basalt melts may need very low water content (<0.46 wt% H_2O) to maintain gravitational stability at the base of the upper mantle. Our results show that the elastic properties of hydrous silicate melts may have important implications for the dynamic evolution and chemical differentiation of the mantle.

1. Introduction

Silicate melts are important carriers of mass and heat in both the crust and mantle, and may have played an important role in controlling chemical differentiation and mass transport in Earth's interior (Agee, 1998; Ohtani and Maeda, 2001; Suzuki and Ohtani, 2003). The density contrast between melts and surrounding solids is a key control on whether a subducting slab floats or sinks through the mantle (Agee and Walker, 1993; Bercovici and Karato, 2003; Stolper et al., 1981; Suzuki et al., 1995). Given the greater compressibility of liquids compared with solids, Stolper et al. (1981) suggested that the density of silicate melts may be higher than that of coexisting solids in the deep upper mantle. The 410-km depth of gravitational stabilization based on seismological observations may be closely related to the density of silicate melts (Revenaugh and Sipkin, 1994).

The viscosity, compressibility, and density of silicate melts are important parameters that influence the migration of magma in Earth's interior (Ai and Lange, 2008; Dingwell, 1998; Hemley, 1998; Matsukage et al., 2005; Rigden et al., 1984; Stolper et al., 1981). Many measurements of silicate melts have been conducted at high pressure–temperature (P–T) conditions. Using shock-wave techniques, Rigden et al. (1984, 1988) directly determined the densities of silicate melts for the first time at high P–T conditions. By using the floating–sinking sphere technique, Agee and Walker (1993) obtained the density of molten komatite and peridotite melts at pressures of between 7 and 10 GPa. These high pressure–temperature experiments can provide constraints on the density of melts, but they are generally limited to low pressures and/or low melt viscosities, and they are also unable to reproduce some elastic properties with pressure (Agee and Walker, 1993; Akins et al., 2004; Mosenfelder et al., 2007, 2009; Rigden et al., 1984, 1988). Brillouin scattering spectroscopy has been widely used to directly measure the sound velocities of silicate glasses and melts, and hence their elastic properties (Sanchez-Valle and Bass, 2010; Tkachev et al., 2005; Whittington et al., 2012). A number of recent

* Corresponding author.
E-mail address: cxgao599@aliyun.com (C.-X. Gao).

http://dx.doi.org/10.1016/j.epsl.2014.09.006
0012-821X/

studies have investigated the structure of silicate glasses and melts using Brillouin scattering, Raman spectroscopy, and NMR, complemented by molecular dynamic simulations (de Koker et al., 2008; Mookherjee et al., 2008; Shim and Catalli, 2009; Tkachev et al., 2005). The pressure-induced structural transitions and the densification mechanism of the silicate glasses have also been extensively studied (Allwardt et al., 2005, 2007; Kelsey et al., 2009; Lee, 2010; Lee et al., 2004, 2011; Park and Lee, 2012; Yarger et al., 1995). Previous high-pressure studies of the structure of silicate melts and glasses suggest that with increasing pressure, Si–O distances increase and bond angles (e.g., for Si–O–Si) decrease in pure SiO_2 glasses (Hemley et al., 1986). The densification of silicate glasses under high pressure occurs by increases in network-forming cation coordination, combined with increases in modifier cation coordination and decreases in mean network bond angles (Allwardt et al., 2005; Lee et al., 2004).

However, few experiments have considered the influence of water on the properties of silicate melts. Water has long been known to play a fundamental role in the igneous processes of Earth's mantle. As the most abundant volatile constituent with low molecular weight, water has a fundamental effect on the physical properties of silicate melts, such as viscosity and density (Malfait and Xue, 2010a; Mysen and Richet, 2005). Numerous experiments have shown that the stability of several hydrous phases at high pressure makes it possible to sequester subducted H_2O at the upper-mantle transition zone and perhaps to the base of the lower mantle (Abe et al., 2000; Agee, 1998; Ohtani and Maeda, 2001; Rigden et al., 1988).

In this paper, the sound velocities and elastic properties of two basalt glasses with different water contents are measured at the pressure of the transition zone (20.0 GPa) by Brillouin scattering spectroscopy in conjunction with a diamond anvil cell (DAC). The density and corresponding elastic parameters are calculated by using the velocity–pressure relationship. Using the bulk velocity–pressure relationship and experimental results on the thermal expansion of the silicate glasses, we estimate the densities of basalt melts with different water contents under upper-mantle pressure. By comparing our calculated densities of basalt melts with previous hydrous mid-ocean ridge basalt (MORB) melts and preliminary reference Earth model (PREM) data, we evaluate the influence of water on the density of hydrous basalt melts and the gravitational stability of basalt melts at a depth of ~410 km.

2. Experimental methods

2.1. Description of samples

The starting materials for our experiment were Feixian high-magnesium basalts erupted during the Early Cretaceous (~120 Ma), and were hand-picked from Huiminzhuang village in Feixian county, eastern China. The basalt samples were fresh and exhibit porphyritic texture and massive structure. The phenocrysts are olivine, clinopyroxene, rare orthopyroxene, and plagioclase (Gao et al., 2008; Pei et al., 2004). Olivine and orthopyroxene xenocrysts are also observed under the microscope. Whole-rock K–Ar dating indicates an Early Cretaceous age of 119 ± 2 Ma for the basalt (Pei et al., 2004). In general, basalt is an ideal candidate for studying mantle silicate melts deep in the mantle (Li and Van Der Hilst, 2010).

The hydrous basalt glasses used during the study were synthesized in a multi-anvil press (YJ-3000t) at the Institute of Geochemistry, Chinese Academy of Sciences, Guiyang, China. The details of this apparatus are contained in Xie et al. (1993). Fig. 1 shows the furnace assembly. A pyrophyllite cube with dimensions of $33 \times 33 \times 33$ mm was used as the pressure medium and was

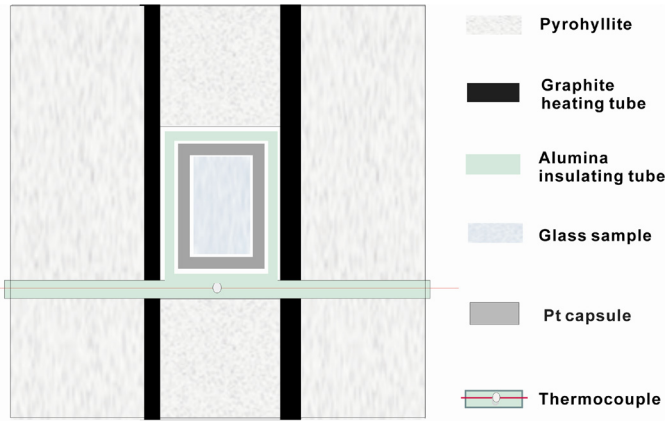

Fig. 1. Schematic diagram of the experimental sample assembly.

heated to 850 °C to remove any absorbed water before the experiment. The original basalt rocks were crushed in a pestle to 200# powder and placed in an oven at 100 °C for >48 h to eliminate any adsorbed water. The powders were sealed in Pt capsules (0.5 mm thick, 6 mm outside diameter, and 6 mm high) with appropriate amounts of water. A graphite heater was wrapped around each Pt capsule and then inserted into a 0.5-mm-thick alumina sleeve. A PtRh10–Pt thermocouple with an estimated accuracy of 5 K was used to measure the temperature. Automatic P–T control was used during the entire experiment. The pressure was maintained at 1 GPa during the synthesis process. Heating was started after the samples had been compressed to the target pressure (1 GPa). The temperature was first raised to 450 °C over 540 s and then maintained for 180 s, then raised to 900 °C over another 540 s and maintained again for 180 s, and then raised to nearly 1400 °C over 680 s. The basalt melts were held at this temperature of nearly 1400 °C for 25 min and then quenched to homogeneous glasses in 20 s with quench rates in the order of 60 K/s. At the end of the run, the heating was switched off but the pressure line was left open to the compressor for 180 s to maintain the nominal run pressure during the quenching process.

The quenched glasses were polished on both sides to attain specimen thicknesses of 100–300 μm. The two samples used in this study were free of crystals and bubbles, as verified by optical microscopy. The chemical composition and homogeneity of the two samples were confirmed by electron microprobe analysis (EMPA) on different points across each glass. Water content was analyzed by Fourier Transform infrared (FTIR) absorption spectroscopy on the same double-sided polished sections. All of the electron microprobe and water content data are given in Table 1. When the total water content of a sample exceeds 2%, the absorption peak of 3550 cm^{-1} (the fundamental OH vibration band) is saturated and cannot be used to determine the total water content. Therefore, in the present study, we used the sum of the infrared absorption peak at 4500 cm^{-1} (OH– groups) and at 5200 cm^{-1} (molecular H_2O) for total water determination (Fig. 2b). The Beer–Lambert law ($c = 1802 \times A/d/\rho/\varepsilon$) is generally used to calculate H_2O content from the FTIR spectrum of minerals, where c is H_2O concentration expressed as a weight fraction (H_2O wt%), A is the height of the absorption peak or integrated area (cm^{-1}) of OH absorption bands in the region of interest, d is the thickness of the specimen in cm, and ε is the molar absorption coefficient of basalt glasses (Ohlhorst et al., 2001).

2.2. Brillouin scattering spectroscopy under high pressure

Two hydrous basalt glasses with different water contents (FX-1 with 0.46 wt% H_2O content and FX-2 with 2.69 wt% H_2O content) and of high optical quality and free of visible inclusions were

Table 1
Electron microprobe (EMP) analyses and Fourier Transform infrared (FTIR) absorption spectroscopy results for two kinds of Feixian basalt glasses.

Sample	SiO_2	TiO_2	Al_2O_3	FeO	MnO	MgO	CaO	Na_2O	K_2O	Cr_2O_3	NiO	Water	OH	H_2O	Total
FX*	48.60	1.09	14.54	9.08	0.12	12.91	8.85	2.31	2.21	0.10	0.06	0	0	0	99.86
FX-1-1	48.18	0.96	14.42	8.23	0.09	12.22	8.88	2.21	2.17	0.08	0.05	0.46	0.16	0.32	98.17
FX-1-2	48.35	1.13	14.41	8.75	0.14	12.10	8.70	2.06	2.16	0.10	0.06	0.46	0.16	0.32	98.41
FX-1-3	48.56	1.14	14.72	8.93	0.10	12.61	8.75	2.09	2.16	0.10	0.10	0.46	0.16	0.32	99.73
FX-1-4	48.21	1.09	15.98	8.54	0.12	12.74	8.63	2.09	2.04	0.12	0.05	0.46	0.16	0.32	100.1
FX-1-5	48.12	1.07	15.93	8.22	0.16	12.42	8.47	2.07	2.06	0.12	0.09	0.46	0.16	0.32	99.19
FX-1#	48.28	1.08	15.09	8.54	0.12	12.41	8.68	2.10	2.12	0.11	0.07	0.46	0.16	0.32	99.11
FX-2-1	48.30	1.01	14.92	7.89	0.14	11.82	8.72	2.10	2.02	0.06	0.06	2.69	0.45	2.24	99.72
FX-2-2	48.59	1.07	14.84	7.75	0.10	12.11	8.74	2.01	2.19	0.12	0.07	2.69	0.45	2.24	100.3
FX-2-3	48.37	0.95	14.07	7.63	0.10	12.05	8.87	2.13	2.09	0.09	0.08	2.69	0.45	2.24	99.11
FX-2#	48.42	1.01	14.61	7.76	0.11	11.99	8.77	2.08	2.10	0.09	0.07	2.69	0.45	2.24	99..7

* The original rock sample.
\# The average values of multiple measurements.

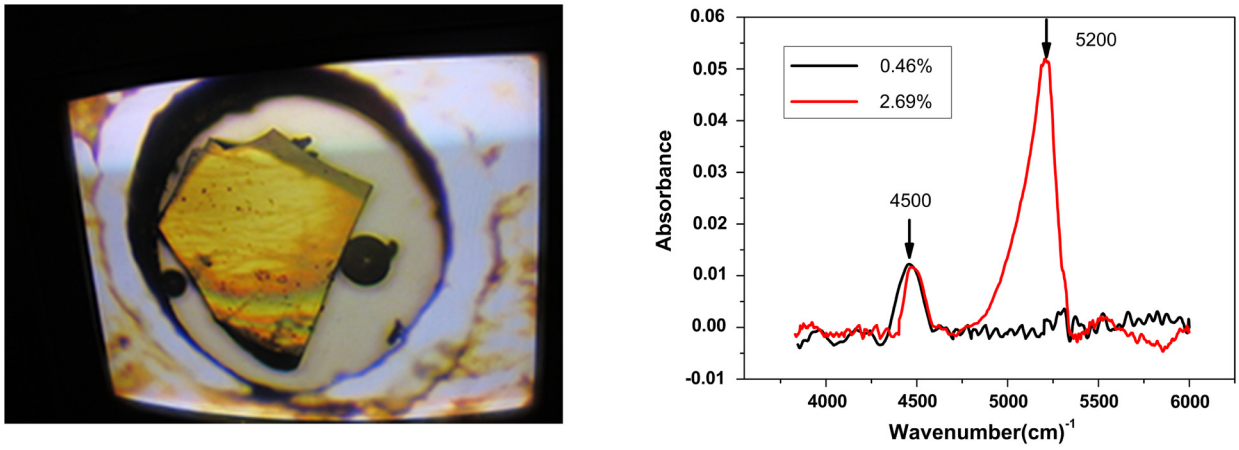

(a) (b)

Fig. 2. (a) A piece of basalt glass sample (40 μm thick) was loaded in the cell together with two ruby spheres at each side of the sample. **(b)** Absorption peaks at 4500 cm^{-1} (OH– groups) and 5200 cm^{-1} (molecular H_2O) of the two basalt glasses.

prepared for Brillouin scattering spectroscopy measurements. The hydrous basalt glasses were polished to a thickness of 40–50 μm and loaded into a gasketed high-pressure Mao–Bell-type DAC with a culet face of 500 μm in diameter, as shown in Fig. 2a. A sheet of T-301 stainless steel was pre-indented to 70–80 μm and drilled with holes 250–300 μm in diameter. In each spectroscopy determination, a piece of basalt glass sample (40 μm thick) was loaded in the cell, together with 2 or 3 ruby spheres (Chervin et al., 2001) for determining pressure using the ruby fluorescence method. Brillouin scattering measurements were conducted using an Argon ion laser ($\lambda_0 = 514.5$ nm) as an excitation source with a $3+3$ pass tandem Fabry–Pérot interferometer designed by Sandercock (Mock et al., 1987). All measurements were conducted in a symmetric scattering geometry, in which the sound velocities, V_i ($i = P$ or S), are directly calculated without knowing the refractive index of the sample, using the relationship (Whitfield et al., 1976): $V_i = \lambda_0 \Delta\omega_i/(2\sin(\theta/2))$, where V_i is the compressional (V_P) or shear (V_S) phonon velocity, ω_i is the measured Brillouin shift, λ_0 is the laser wavelength (514.5 nm), and θ is the angle between the incident and scattered light outside the sample platelet (60°). Because of the overlap of the peak position of the sample and the pressure-transmitting medium, we used either a methanol–ethanol (ME) mixture (4:1 volume ratio) or cryogenically loaded Ar as the pressure-transmitting medium. To avoid the possibility of relaxation of the glass, each sample was held at each pressure used for at least 5–6 h before Brillouin spectra were collected. For each pressure, at least three different spots on each sample were measured to confirm the homogeneity of the sample. The experimental error of multiple measurements for each sample was less than 0.1%, so we consider the weighted mean value as a reliable representation of the data for each sample. Laser power ranged from 10 to 100 mW and the collection times ranged from 10 min to 10 h depending on the pressure used.

2.3. Thermal expansion coefficients of the basalt glasses

The thermal expansion of each glass was measured with a horizontal-type dilatometer (DIL402C, Netzsch). Because the hydrous basalt glasses were synthesized under a pressure of 1 GPa, directly measuring the thermal expansion of samples was unrealistic. Previous studies have demonstrated that performing thermal expansion measurements on compressed glasses gives spurious results, whereby the observed expansion is a combination of the true thermal expansion and the temperature-induced release of the permanent densification (Bouhifd et al., 2001). Therefore, measurements over a series of heating–cooling experiments up to T_g (glass transition temperature) and back down are necessary to obtain the relaxed thermal expansion.

To overcome the problem of the permanent densification of the original compressed glasses, measurements of the thermal expansion coefficient for each hydrous glass were divided into two stages, for which the temperature–time path is shown in Fig. 3a. In the first stage, the initially compacted glass was heated continuously from room temperature to T_1 (Fig. 3a), which is slightly lower than its transition temperature T_g (T_g was established from our previous thermal expansion experiments) and was maintained at T_1 for 180 min. Then the temperature was raised to T_2 (the

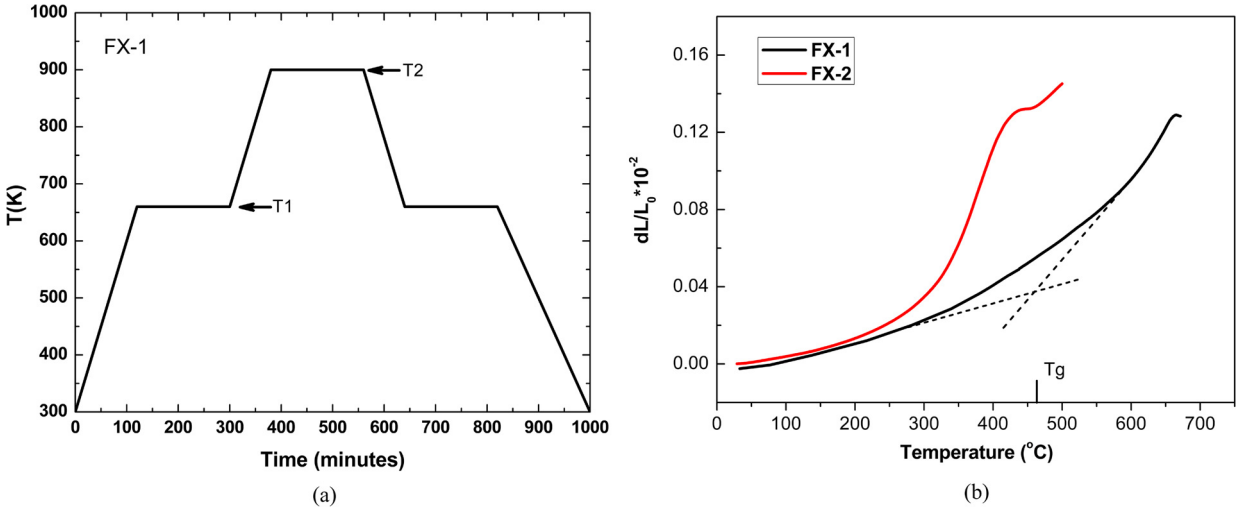

Fig. 3. **(a)** Typical temperature–time path for hydrous basalt samples, in this case of FX-1, where T_1 indicates a temperature that is slightly lower than its transition temperature T_g and T_2 indicates a temperature that is higher than T_g. **(b)** dL/L_0 curves of the hydrous basalt melts obtained with the DIL402C dilatometer at a heating rate of 3 K/min. The slope of the curve between 25 °C and the point where the slope diverges from a straight line was used to calculate the coefficient of thermal expansion of each glass. T_g (FX-1) = 327 °C and T_g (FX-2) = 457 °C.

highest temperature) and maintained for 180 min. Finally, the temperature was decreased to T_1 and maintained for another 180 min. The phases of temperature increase and decrease during the procedure were applied at a constant rate of 3 K/min. After the first density measurement of each compacted glass, we measured the density of the relaxed glass and performed a second measurement with the same heating rate on the relaxed sample. No density variations were observed after the second measurement.

Fig. 3b shows the dL/L_0 (L_0 is the initial length of the sample) curves of the hydrous basalt glasses obtained from scanning dilatometry. The linear thermal expansion coefficient is calculated as the relative change in the length of the sample across a temperature interval (ΔT):

$$\alpha_{\text{linear}} = (1/L_0)(\partial L/\partial T). \quad (1)$$

Because of the isotropy of the glasses, the volume thermal expansion coefficient (α_{volume}) is three times higher than the linear expansion coefficient (α_{linear}). It should be noted that the change in volume thermal expansion both before and after the glass transition temperature shows an almost linear trend (Fig. 3b). The coefficient of volume thermal expansion of each glass or melt was determined by measuring the slope of the dilatometry data both before and after T_g.

3. Results and discussion

3.1. Brillouin spectra and the sound velocities of the basalt glasses at pressures of up to 20 GPa

The compressional and shear wave sound velocities of the two basalt glasses measured at ambient pressure are $V_{P(FX\text{-}1)} = 6880 \pm 25$ m/s and $V_{S(FX\text{-}1)} = 3825 \pm 20$ m/s, and $V_{P(FX\text{-}2)} = 6742 \pm 31$ m/s and $V_{S(FX\text{-}2)} = 3760 \pm 21$ m/s, respectively. The wave sound velocities (V_P and V_S) of the hydrous glasses in our experiment are slightly higher than the values reported by Malfait et al. (2011) ($V_P = 6416 \pm 27$ to 6380 ± 23 m/s and $V_S = 3636 \pm 31$ to 3589 ± 17 m/s for <0.18 mol% to 13.68 mol% H_2O content, synthesized at 25 MPa) and Whittington et al. (2012) ($V_P = 6505$ to 6330 m/s and $V_S = 3711$ to 3576 m/s for 0 mol% to 9.61 mol% H_2O content, synthesized at 0.1–215 MPa). This may be attributed to the higher synthesis pressure (1 GPa) used for our hydrous basalt glasses, which is also reflected by their higher densities.

The densities of the basalt glasses at room pressure were measured using the Archimedean method, as reported in Table A (see Appendix A) and with an error of <0.5%. Fig. 4 shows a representative Brillouin spectra of FX-1 glass under high pressure using Ar and ME as the pressure-transmitting mediums. For each pressure, the spectra are of good quality with a high signal-to-noise ratio, and the pronounced feature at the center of each spectrum is the elastic scattered light signal (Rayleigh scattering). The variables ω_P, ω_S, ω_{Ar}, and ω_{ME} represent the Brillouin shifts of the compressional and shear wave sound velocities (V_P and V_S) of the glass, and of the Ar and ME pressure-transmitting mediums, respectively. As seen in the 4.73 GPa spectrum of Fig. 4a, because of the peak overlap we were unable to determine the shear Brillouin shift ω_S of the glass loaded in the Ar pressure-transmitting medium. For the 7.07, 7.85, and 9.05 GPa spectra of Fig. 4b, the compressional Brillouin shifts ω_P of the sample were covered by the ME vibration peak. In fact, in all cases there are several blank areas for the vibration peaks of the sample under particular pressure-transmitting mediums (e.g., for the sample under the Ar pressure-transmitting medium, the pressure range from 2.2 to 5.8 GPa is invalid for the compression process and from 5.1 to 10.2 GPa for the decompression process). Therefore, we used both Ar and the ME mixture (4:1 volume ratio) as pressure-transmitting mediums. In the overlap range of the Ar and ME pressure-transmitting mediums, the sound velocities obtained are found to be in excellent agreement.

Fig. 5 shows the sound velocities of FX-1 and FX-2 as a function of pressure during both the compression and decompression processes. V_P and V_S vary widely during both compression and decompression. For FX-1 glass upon compression, the first apparent change in the slope of the pressure dependence of both V_P and V_S is at around 7.1 GPa, suggesting a possible amorphous to amorphous transition (Tkachev et al., 2005). Both V_P and V_S of FX-1 glass increase gradually from ambient pressure to 7.1 GPa, followed by a higher rate of increase above this pressure. This sharp change in sound velocity with respect to pressure is also observed in other silicate or pure silica glasses (Grimsditch, 1984; Sanchez-Valle and Bass, 2010). From 7.1 GPa to about 11.9 GPa, the rates of increase in both V_P and V_S reduce, and then monotonically increase with increasing pressure from 11.9 GPa up to the highest pressure. During the decompression process, both V_P and V_S follow a path that differs from the compression process, exhibiting a smooth decrease with decreasing pressure. The velocities during decompression remain higher than those during

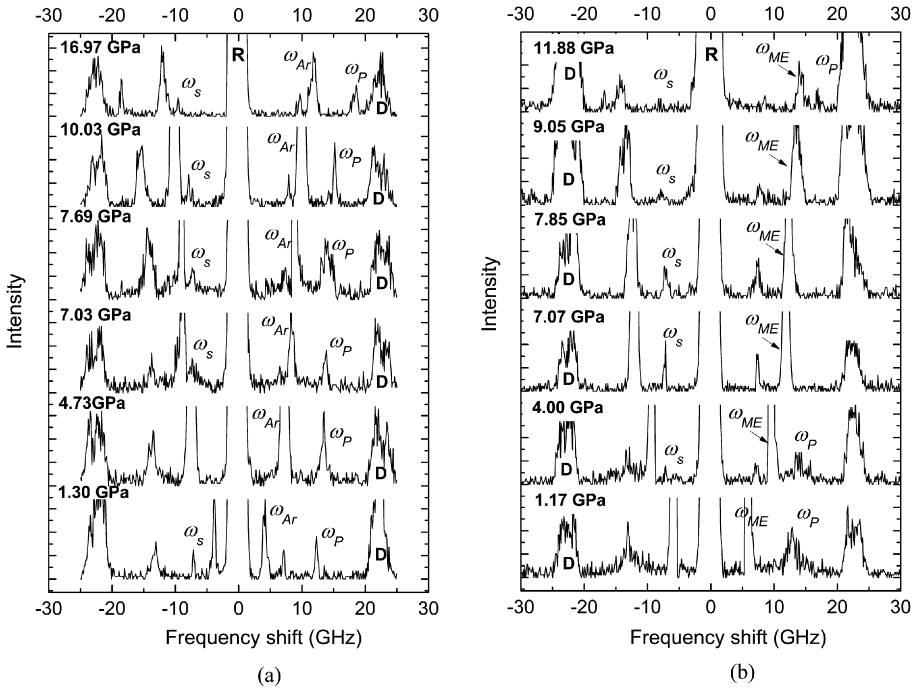

Fig. 4. (a) and **(b)**: Selected Brillouin scattering spectra of Feixian basalt glasses (FX-1 and FX-2) collected at different pressures in Ar and ME pressure-transmitting mediums. R is the Rayleigh scattering component, D refers to diamond peak. The variables ω_P, ω_S, ω_{Ar}, and ω_{ME} represent the Brillouin shifts corresponding to the frequencies of the compressional and shear acoustic modes of the glass and the Ar and ME pressure-transmitting mediums, respectively.

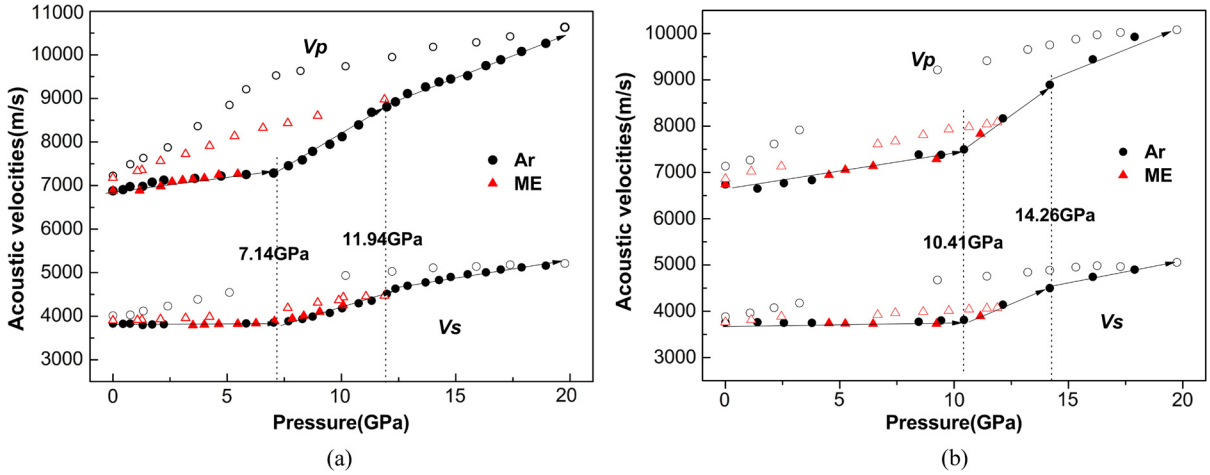

Fig. 5. Pressure dependence of V_P and V_S of FX-1 (**a**) and FX-2 (**b**) glasses during compression (solid symbols) and decompression (open symbols) runs. Errors in velocities and pressures are smaller than the size of the symbols.

compression over the entire pressure range, and V_P and V_S after complete decompression are slightly higher than those obtained before pressurization. This may be attributed to a permanent densification of the silicate glass, which is a common feature of silicate glasses under high pressure (Gaudio et al., 2008; Lee et al., 2008; Shim and Catalli, 2009). The structural rearrangements in melts become kinetically impeded in the glass transition, and eventually the structure of the liquid is permanently imparted into the glass, and only the purely elastic part of the compression is able to be released after decompression (Seifert and Moldowan, 1981; Tammann and Jenckel, 1929). The pressure dependence of the velocities of the FX-2 glass is similar to that of the FX-1 glass except for the delay in the first and second points of change in slope, which occur at higher pressures of around 10.5 and 14.3 GPa, respectively (Fig. 5b). The initial velocities of FX-2 glass are slightly lower than those of FX-1, which can be attributed to the higher water content of FX-2 glass. At the highest pressure used in this study, the differences between V_P and V_S for FX-1 and FX-2 glasses are 553 ± 21 and 157 ± 25 m/s, respectively.

3.2. Elastic properties of the basalt glasses with different water contents

The points of change in slope in V_P and V_S indicate that the basalt glasses undergo significant structural modifications at particular pressures. However, the order of the transitions depend on the presence of discontinuities in thermodynamic quantities. The Brillouin scattering geometry used in this study is forward symmetric, which allows elastic properties and density to be measured without knowing the refractive index of glass under high pressure. Therefore, the density of the glass can be calculated using the following equation:

$$dP/d\rho = V_P^2 - 4V_S^2/3. \quad (2)$$

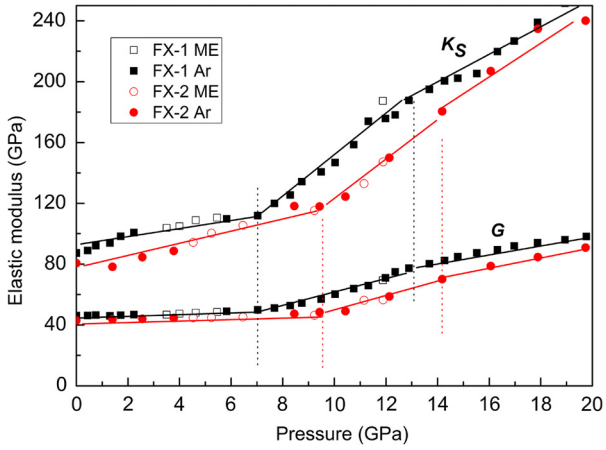

Fig. 6. Pressure dependence of the aggregate elastic moduli of FX-1 and FX-2 basalt glasses upon compression. The full lines are linear fits to the experimental values. The vertical dashed lines represent transition points of FX-1 and FX-2.

Integrating Eq. (2), we obtain:

$$\rho - \rho_0 = \int_{P_0}^{P} \frac{1}{V_P^2 - 4V_S^2/3} dP. \tag{3}$$

The initial density (ρ_0) was measured under ambient conditions. Given the velocities at each pressure, we obtained the density at each pressure using Eq. (3). All of the velocity data under Ar and ME conditions (including the use of mean values of velocity in the overlap area of Ar and ME) were integrated to calculate the density of each glass. The adiabatic shear (G), adiabatic bulk modulus (K_S), and adiabatic compressibility (β_S) of these silicate glasses were calculated using the relationships of $G = \rho V_S^2$, $K_S = \rho(V_P^2 - 4/3V_S^2)$, and $\beta_S = 1/K_S$. The calculated values of ρ, G, K_S, and β_S are listed in Table A (see Appendix A).

Fig. 6 shows the pressure dependence of the calculated elastic parameters. The monotonic increase in density shown in Fig. 7, together with the sudden changes in elastic modulus slope with respect to pressure, is in accordance with the characteristics of a second-order phase transition. Because melts lack long-range order and contain large variations in both bond lengths and angles, abrupt increases in density with increasing pressure are unlikely. For the FX-1 glass at pressures of <7.1 GPa, $(\partial K_S/\partial P)_T = 1.2 \pm 0.2$ and $(\partial G/\partial P)_T = 0.13 \pm 0.1$. At pressures of >7.1 GPa, both K_S and G show a higher rate of increase, $(\partial K_S/\partial P)_T = 5.2 \pm 0.3$ and $(\partial G/\partial P)_T = 4.1 \pm 0.3$. A less dramatic change in the slope of the pressure–elastic modulus curve is seen at a pressure of about 13.0 GPa (Fig. 6). These different rates of increase in modulus with respect to pressure indicate different densification mechanisms for different pressure regions. The second-order phase transition observed in FX-1 at 7.1 GPa cannot be attributed to recrystallization or disproportionation because the glass remained isotropic during the experiment and no crystals were detected in the recovered sample by inspection under polarized light.

Many models and experiments have been used to explain the continuous change in density in conjunction with anomalous (sharp) changes in the slope of the elastic modulus (Allwardt et al., 2007; Gaudio et al., 2008; Lee et al., 2004, 2011; Shim and Catalli, 2009; Stolper and Ahrens, 1987; Yarger et al., 1995). With increasing pressure, the T–O (T = Si, Al; i.e., a tetrahedrally coordinated cation) distance increases and bond angles (e.g. T–O–T) decrease, and the changes in these internal variables evidently intensify the topological disorder, resulting in distortion of network polyhedra and reorganization of the oxygen network (Allwardt et al., 2005, 2007; de Koker et al., 2008; Kelsey et al., 2009; Lee and Stebbins, 2000). In addition, the change in the distribution of chemical ordering would elevate the fraction of highly coordinated Si and Al in partially depolymerized melts (Lee et al., 2004). In fact, at higher pressures, Al tends to be more highly coordinated than does Si, which specifically forms $^{[4]}$Si–O–$^{[5,6]}$Al (Lee et al., 2004, 2011). The abrupt nature of the variation in both V_P and V_S with respect to pressure can be attributed to the topological rearrangement of the silicate network to high [Si, Al]–O coordination. At pressures of <7.1 GPa, both K_S and G increase gradually whereas density increases at a high rate, indicating a reduction in the free volume of $^{[4]}$Si and $^{[4]}$Al caused by the decrease in bond angle only, without any emergence of $^{[5,6]}$[Si, Al]. At pressures of >7.1 GPa, the decrease in bond angle becomes difficult, consistent with the sharp drop in compressibility and slow increase in density of the glass. This second-order transition ends at about 13.0 GPa, where another anomalous change in modulus is observed. In short, the major mechanism of pressure-induced structural changes is the result of the decrease in the configurational enthalpy and entropy of the silicate melts (Lee and Stebbins, 2003).

For FX-2 glass, both K_S and G exhibit similar variational tendencies to those of FX-1, except for the delay in the structural transition points in FX-2. Comparing the elastic modulus of FX-2 with that of FX-1, for pressures up to 10 GPa at 300 K, the additional 2.23 wt% H_2O of FX-2 lowers the Ks and G of FX-2 by 10%–17% and 13%–18%, respectively. However, the additional 2.23 wt% H_2O does not affect the pressure derivatives of the elastic moduli of FX-2 basalt glass compared with FX-1. The second-order transition for FX-2 occurs at around 10 GPa, which is 3 GPa higher than in the case of FX-1. This means that water content has a significant effect on the elastic properties of the silicate system of the glasses. Previous studies have suggested that the densification of silicate glasses can be facilitated by increases in network-forming cation coordination, combined with increases in modifier cation coordination and decreases in mean network bond angles (Allwardt et al., 2005). With an increase in pressure, the proportion of nonbridging oxygen (NBO) ions gradually decreases, resulting in the formation of new oxygen clusters that include 5- and 6-coordinated Si and Al in addition to 4-coordinated Al and Si, such as $^{[4]}$Si–O–$^{[5,6]}$Si, $^{[4]}$Si–O–$^{[5,6]}$Al and (K, Na)–O–$^{[5,6]}$Si (Lee et al., 2004, 2011). For hydrous silicate melts, it is generally considered that water can interact with the bridging oxygen of T–O tetrahedrons and finally decrease the degree of polymerization of the silicate melts (Lee et al., 2011). The process can be described as follows:

$$\equiv\text{T–O–T}\equiv + \text{H}_2\text{O} \Leftrightarrow 2\equiv\text{T–OH}. \tag{4}$$

Previous studies demonstrate that the pressure-induced coordination change is closely related to the NBO/T ratio of the melts (Kelsey et al., 2009; Lee, 2010; Lee et al., 2004). However, the correlation of coordination with NBO/T is not a simple linear trend, but rather a function of competing densification mechanisms involving steric hindrance due to the fraction of network-modifying cations and NBOs in the silicate melts (Lee et al., 2011). Highly coordinated T (Si, Al) is formed at the expense of NBO ions, whereas the increase in network-modifying cations will lead to an increase in steric hindrance and thus prohibit the coordination transformation. The NBO/T ratios of FX-1 and FX-2 were calculated to be 0.92 and 1.09, respectively. This means that the excess water content of FX-2 will interact with more network-forming cations and create Si–OH and Al–OH groups, in addition to forming molecular water (Malfait and Xue, 2010a, 2010b). The addition of non-network-forming cations around NBO ions would prohibit NBO ions from being connected to other nearby framework cations (i.e.,$^{[5,6]}$(Si, Al)); this steric hindrance becomes dominant and eventually results in the hysteresis of the second-order phase transition (Malfait et al., 2011; Malfait et al., 2014; Malfait and Xue, 2010a, 2010b).

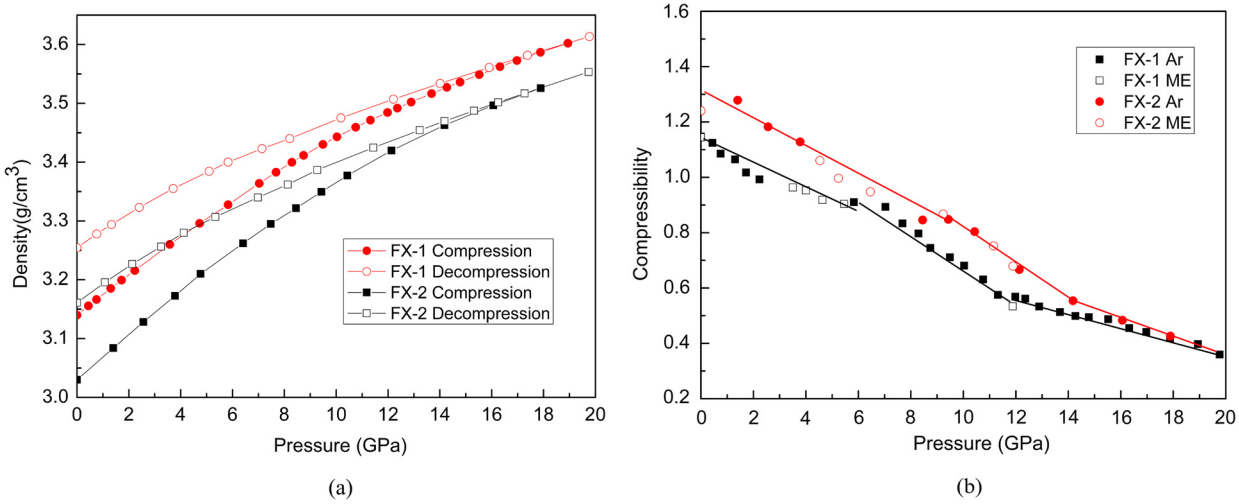

Fig. 7. (a) Density of FX-1 and FX-2 glasses as a function of pressure on compression (full symbols) and decompression (open symbols) experiments. Estimated errors on density (0.5%) are smaller than the symbol size. (**b**) Pressure dependence of compressibility of FX-1 and FX-2 glasses upon compression.

This lagging behavior of the silicate melts can be also manifested by Raman experiments on Mg silicate glass (Shim and Catalli, 2009). The frequencies of stretching vibrations are related to the degree of polymerization of the SiO_4 tetrahedral network: the tetrahedra with zero (Q^0), one (Q^1), two (Q^2), and three (Q^3) bridging oxygen ions are associated with modes at 850, 900, 950–1000, and 1050–1100 cm^{-1}, respectively (Mysen and Richet, 2005). A tetrahedra model with a less polymerized Si–O network can remain stable at higher pressure than can other stretching modes. When the structure of the glass is depolymerized, increasing the coordination of [Si, Al] is more difficult, which is also consistent with the model of Stolper and Ahrens (1987). Consequently, the higher transition pressure of FX-2 can be attributed to the relative deficiency of highly polymerized SiO_4 tetrahedra. In other words, water makes it difficult for Si to transform from a lower to a higher coordination. The transition pressure is sensitive to the degree of polymerization of the Si–O network, leading to higher transition pressures in glasses with low Si concentrations and abundant network modifier cations.

3.3. Density and compressibility

Fig. 7a displays the calculated densities of FX-1 and FX-2 glasses during both compression and decompression. Unlike the sharp changes in the slopes of velocities and elastic modulus with respect to pressure under compression, the densities of FX-1 and FX-2 glasses increase smoothly with increasing pressure and the final values (at 20.0 GPa) are 3.61 and 3.56 g/cm^3, respectively. The densities during decompression are always higher than those during compression at the same pressure. As pressure is returned to ambient conditions, the densities of FX-1 and FX-2 do not return to their initial values. The decompressed FX-1 and FX-2 glasses are 3.5% and 4.3% denser compared with the glasses prior to compression, respectively. This densification effect in basalt glasses has been observed in previous experimental studies of silicate glasses (Sanchez-Valle and Bass, 2010; Tkachev et al., 2005).

It is interesting to note that before pressurization, the density of FX-1 is higher than that of FX-2 (Fig. 7a), indicating that water content reduces the density of the system. The compressibility of glasses FX-1 and FX-2 decreases steeply with pressure and FX-2 (with higher water content) exhibits greater compressibility than does FX-1 under compression (Fig. 7b). Similar to the velocities, the compressibility also shows sharp changes at both the beginning and the end of the second-order transition. In silicate glasses and melts, water can break and replace the bridging oxygen of the Si–O tetrahedron and increase the number of NBO ions (Kohn, 2000; Malfait et al., 2011; Malfait and Xue, 2010a, 2010b; Mysen and Richet, 2005; Mysen et al., 2009). The breaking of the stable tetrahedral bridging oxygen structure can make the silicate structure more easily compressed. Because of the reduction in the number of bridging oxygens, the change in (Si, Al) coordination from a lower level (4) to a higher level (5 or 6) becomes difficult, which delays the onset of the second-order transition in FX-2 glass. After the transition, the difference between the compressibilities of FX-1 and FX-2 decreases and tends to vanish with increasing pressure. Before the second-order transition, water reduces the density of hydrous basalt glass and softens the silicate structure. After the transition, with the increase in higher (Si, Al) coordination, the effect of water on density becomes weak, and the compressibility of the two glasses tends to overlap.

3.4. Density of hydrous basalt melts at the base of Earth's upper mantle

To evaluate the gravitational stability of hydrous basalt melts at the base of Earth's upper mantle, we considered the thermal expansion of our glasses with respect to the densities of basalt melts. Fig. 3b shows that higher water content leads to higher thermal expansion coefficients but reduces the glass transition temperature. However, the ambient pressure thermal expansion coefficient is insufficient on its own to predict the density of melts because the thermal expansion coefficient of solids could be significantly reduced at high pressures (Chopelas and Boehler, 1989; Suzuki et al., 1998). Therefore, we used an approximate relationship between thermal expansion coefficient of solid and pressure to determine the thermal expansion coefficients of basalt melts under high pressure (Guillermet, 1986; Yan, 2000):

$$\alpha(T,P)=\alpha(T,0)\left[1-\frac{P}{K_0+(K_0'+1)P/2}\right]^{\delta_T(T,0)} \tag{5}$$

where $\alpha(T,0)$ is the thermal expansion coefficient of melts at ambient pressure, and K_0 and K_0' are the isothermal bulk modulus and its first-order pressure derivative at ambient conditions, respectively, and $\delta(T,0)$ is the isothermal Anderson–Grüneisen parameter at ambient pressure, calculated as follows:

$$\delta_T(T,0)=-\frac{1}{\alpha K_T}\left(\frac{\partial K_T}{\partial T}\right) \tag{6}$$

where $\partial K_T/\partial T$ is the first-order partial derivative of the bulk modulus with temperature. In the present study, we chose $K_0=$

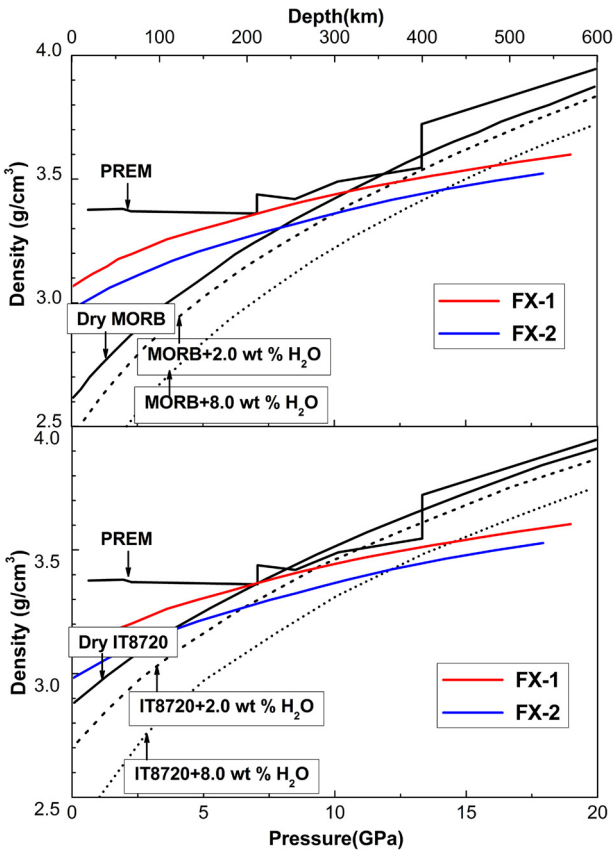

Fig. 8. Densities of hydrous basalt melts corresponding to the compositions of FX-1 and FX-2 versus hydrous MORB melts and PREM. The densities of MORB melts and IT8720 are from Sakamaki et al. (2006). The data for PREM are from Dziewonski and Anderson (1981).

40.0 GPa, $K_0' = 5.0 \pm 0.7$, and $(\partial K_T/\partial T) = -74$ GPa/K from a previous experimental study (Ohtani and Maeda, 2001) in which the sample used was similar to our basalt glasses. Finally, we obtained the densities of FX-1 and FX-2 hydrous basalt melts at high pressure and high temperature as displayed in Fig. 8.

The resulting density curves of our hydrous basalt melts versus those of previous hydrous MORB melts (Sakamaki et al., 2006) and PREM data are shown in Fig. 8. For depths to 200 km, the densities of our hydrous basalt melts are higher than that of dry MORB. At a depth of 300 km, the density of the hydrous basalt melt with 2.69 wt% water is equal to that of MORB with 2.0 wt% water. At a depth of 200 km, the density of the hydrous basalt melt with 0.46 wt% water is equal to that of PREM (Dziewonski and Anderson, 1981) but at 400 km is slightly lower than that of PREM. This means that basalt melts containing 0.46 wt% water would be unstable at the 410-km discontinuity. Sakamaki et al. (2006) proposed that the hydrous IT8720 composition (Ito and Takahashi, 1987; Suzuki et al., 1995) is a good candidate for the partial melt at the base of the upper mantle. Therefore, we compare the densities of hydrous basalt melts with the hydrous IT8720 composition in Fig. 8b, which shows that at a depth of about 200 km, the density of our hydrous basalt melt with 2.69 wt% water is equal to that of the IT8720 composition with 2.0 wt% water content. With increasing depth, the density contrast between our hydrous basalt melt (FX-1) and the hydrous IT8720 composition (2.0 wt% water content) gradually increases and reaches 0.1 g/cm^3 at 410 km depth.

Although relevant density data for dry basalt melts are not available, the density differences of our hydrous basalt melts with PREM and MORB illustrate that the basalt melts would need to contain very low water contents (<0.46 wt%) to guarantee their gravitational stability at the bottom of the upper mantle. The dry mantle transition zone model constructed by Yoshino et al. (2008) suggests that Earth's mantle transition zone might store very little water (<0.1 wt%), which is consistent with our experimental results.

Acknowledgements

We thank Professor Qun-ke Xia for technical support on the electron microprobe and infrared absorption spectroscopy experiments. We also thank Professor Qiong Liu for hospitality and stimulating discussion. This work was supported by the National Basic Research Program of China (Grant No. 2011CB808204), the National Natural Science Foundation of China (Grant Nos. 91014004, 11374121, and 11074094), China Postdoctoral Science Foundation (Grant No. 2013M540243), and the Fundamental Research Funds for Jilin University, China (Grant No. 450060491500).

Appendix A. Supplementary material

Supplementary material related to this article can be found online at http://dx.doi.org/10.1016/j.epsl.2014.09.006.

References

Abe, Y., Ohtani, E., Okuchi, T., Righter, K., Drake, M., 2000. Water in the early Earth. Orig. Earth Moon 1, 413–433.
Agee, C.B., 1998. Crystal–liquid density inversions in terrestrial and lunar magmas. Phys. Earth Planet. Inter. 107, 63–74.
Agee, C.B., Walker, D., 1993. Olivine flotation in mantle melt. Earth Planet. Sci. Lett. 114, 315–324.
Ai, Y., Lange, R.A., 2008. New acoustic velocity measurements on CaO–MgO–Al_2O_3–SiO_2 liquids: reevaluation of the volume and compressibility of $CaMgSi_2O_6$–$CaAl_2Si_2O_8$ liquids to 25 GPa. J. Geophys. Res. Solid Earth (1978–2012) 113, 1978–2012.
Akins, J.A., Luo, S.N., Asimow, P.D., Ahrens, T.J., 2004. Shock-induced melting of $MgSiO_3$ perovskite and implications for melts in Earth's lowermost mantle. Geophys. Res. Lett. 31 (14).
Allwardt, J.R., Stebbins, J.F., Schmidt, B.C., Frost, D.J., Withers, A.C., Hirschmann, M.M., 2005. Aluminum coordination and the densification of high-pressure aluminosilicate glasses. Am. Mineral. 90, 1218–1222.
Allwardt, J.R., Stebbins, J.F., Terasaki, H., Du, L.-S., Frost, D.J., Withers, A.C., Hirschmann, M.M., Suzuki, A., Ohtani, E., 2007. Effect of structural transitions on properties of high-pressure silicate melts: ^{27}Al NMR, glass densities, and melt viscosities. Am. Mineral. 92, 1093–1104.
Bercovici, D., Karato, S.-i., 2003. Whole-mantle convection and the transition-zone water filter. Nature 425, 39–44.
Bouhifd, A.M., Whittington, A., Richet, P., 2001. Partial molar volume of water in phonolitic glasses and liquids. Contrib. Mineral. Petrol. 142, 235–243.
Chervin, J., Canny, B., Mancinelli, M., 2001. Ruby-spheres as pressure gauge for optically transparent high pressure cells. High Press. Res. 21, 305–314.
Chopelas, A., Boehler, R., 1989. Thermal expansion measurements at very high pressure, systematics, and a case for a chemically homogeneous mantle. Geophys. Res. Lett. 16, 1347–1350.
de Koker, N., Stixrude, L., Karki, B.B., 2008. Thermodynamics, structure, dynamics, and freezing of Mg_2SiO_4 liquid at high pressure. Geochim. Cosmochim. Acta 72, 1427–1441.
Dingwell, D.B., 1998. Melt viscosity and diffusion under elevated pressures. Rev. Mineral. Geochem. 37, 397–424.
Dziewonski, A.M., Anderson, D.L., 1981. Preliminary reference Earth model. Phys. Earth Planet. Inter. 25, 297–356.
Gao, S., Rudnick, R.L., Xu, W.-L., Yuan, H.-L., Liu, Y.-S., Walker, R.J., Puchtel, I.S., Liu, X., Huang, H., Wang, X.-R., 2008. Recycling deep cratonic lithosphere and generation of intraplate magmatism in the North China Craton. Earth Planet. Sci. Lett. 270, 41–53.
Gaudio, S.J., Sen, S., Lesher, C.E., 2008. Pressure-induced structural changes and densification of vitreous $MgSiO_3$. Geochim. Cosmochim. Acta 72, 1222–1230.
Grimsditch, M., 1984. Polymorphism in amorphous SiO_2. Phys. Rev. Lett. 52, 2379–2381.
Guillermet, A.F., 1986. The pressure dependence of the expansivity and of the Anderson–Grüneisen parameter in the Murnaghan approximation. J. Phys. Chem. Solids 47, 605–607.
Hemley, R.J., 1998. Ultrahigh-Pressure Mineralogy: Physics and Chemistry of the Earth's Deep Interior. Mineralogical Society of America, Washington, DC.

Hemley, R., Mao, H., Bell, P., Mysen, B., 1986. Raman spectroscopy of SiO_2 glass at high pressure. Phys. Rev. Lett. 57, 747.
Ito, E., Takahashi, E., 1987. Melting of peridotite at uppermost lower-mantle conditions. Nature 328, 514–517.
Kelsey, K.E., Stebbins, J.F., Singer, D.M., Brown Jr, G.E., Mosenfelder, J.L., Asimow, P.D., 2009. Cation field strength effects on high pressure aluminosilicate glass structure: multinuclear NMR and La XAFS results. Geochim. Cosmochim. Acta 73, 3914–3933.
Kohn, S., 2000. The dissolution mechanisms of water in silicate melts; a synthesis of recent data. Mineral. Mag. 64, 389–408.
Lee, S.K., 2010. Effect of pressure on structure of oxide glasses at high pressure: insights from solid-state NMR of quadrupolar nuclides. Solid State Nucl. Magn. Reson. 38, 45–57.
Lee, S.K., Stebbins, J.F., 2000. The structure of aluminosilicate glasses: high-resolution ^{17}O and ^{27}Al MAS and 3QMAS NMR study. Ber. Bunsenges. Phys. Chem. 104, 4091–4100.
Lee, S.K., Stebbins, J.F., 2003. The distribution of sodium ions in aluminosilicate glasses: a high-field ^{23}Na MAS and 3Q MAS NMR study. Geochim. Cosmochim. Acta 67, 1699–1709.
Lee, S.K., Cody, G.D., Fei, Y., Mysen, B.O., 2004. Nature of polymerization and properties of silicate melts and glasses at high pressure. Geochim. Cosmochim. Acta 68, 4189–4200.
Lee, S.K., Lin, J.-F., Cai, Y.Q., Hiraoka, N., Eng, P.J., Okuchi, T., Mao, H.-k., Meng, Y., Hu, M.Y., Chow, P., 2008. X-ray Raman scattering study of $MgSiO_3$ glass at high pressure: implication for triclustered $MgSiO_3$ melt in Earth's mantle. Proc. Natl. Acad. Sci. USA 105, 7925–7929.
Lee, S.K., Yi, Y.S., Cody, G.D., Mibe, K., Fei, Y., Mysen, B.O., 2011. Effect of network polymerization on the pressure-induced structural changes in sodium aluminosilicate glasses and melts: ^{27}Al and ^{17}O solid-state NMR study. J. Phys. Chem. C 116, 2183–2191.
Li, C., Van Der Hilst, R.D., 2010. Structure of the upper mantle and transition zone beneath Southeast Asia from traveltime tomography. J. Geophys. Res. Solid Earth (1978–2012) 115.
Malfait, W.J., Xue, X., 2010a. The nature of hydroxyl groups in aluminosilicate glasses: quantifying Si–OH and Al–OH abundances along the SiO_2–$NaAlSiO_4$ join by ^{1}H, ^{27}Al–^{1}H and ^{29}Si–^{1}H NMR spectroscopy. Geochim. Cosmochim. Acta 74, 719–737.
Malfait, W.J., Xue, X., 2010b. The partial ^{1}H NMR spectra of Al–OH and molecular H_2O in hydrous aluminosilicate glasses: component-resolved analysis of ^{27}Al–^{1}H cross polarization and ^{1}H spin-echo MAS NMR spectra. Solid State Nucl. Magn. Reson. 37, 60–68.
Malfait, W.J., Sanchez-Valle, C., Ardia, P., Médard, E., Lerch, P., 2011. Amorphous materials: properties, structure, and durability compositional dependent compressibility of dissolved water in silicate glasses. Am. Mineral. 96, 1402–1409.
Malfait, W.J., Seifert, R., Petitgirard, S., Mezouar, M., Sanchez-Valle, C., 2014. The density of andesitic melts and the compressibility of dissolved water in silicate melts at crustal and upper mantle conditions. Earth Planet. Sci. Lett. 393, 31–38.
Matsukage, K.N., Jing, Z., Karato, S.-i., 2005. Density of hydrous silicate melt at the conditions of Earth's deep upper mantle. Nature 438, 488–491.
Mock, R., Hillebrands, B., Sandercock, R., 1987. Construction and performance of a Brillouin scattering set-up using a triple-pass tandem Fabry–Pérot interferometer. J. Phys. E, Sci. Instrum. 20, 656.
Mookherjee, M., Stixrude, L., Karki, B., 2008. Hydrous silicate melt at high pressure. Nature 452, 983–986.
Mosenfelder, J.L., Asimow, P.D., Ahrens, T.J., 2007. Thermodynamic properties of Mg_2SiO_4 liquid at ultra-high pressures from shock measurements to 200 GPa on forsterite and wadsleyite. J. Geophys. Res. Solid Earth (1978–2012) 112.
Mosenfelder, J.L., Asimow, P.D., Frost, D.J., Rubie, D.C., Ahrens, T.J., 2009. The $MgSiO_3$ system at high pressure: thermodynamic properties of perovskite, postperovskite, and melt from global inversion of shock and static compression data. J. Geophys. Res. 114, B01203.
Mysen, B., Richet, P., 2005. Silicate Glasses and Melts: Properties and Structure. Elsevier.
Mysen, B.O., Fogel, M.L., Morrill, P.L., Cody, G.D., 2009. Solution behavior of reduced C–O–H volatiles in silicate melts at high pressure and temperature. Geochim. Cosmochim. Acta 73, 1696–1710.
Ohlhorst, S., Behrens, H., Holtz, F., 2001. Compositional dependence of molar absorptivities of near-infrared OH– and H_2O bands in rhyolitic to basaltic glasses. Chem. Geol. 174, 5–20.
Ohtani, E., Maeda, M., 2001. Density of basaltic melt at high pressure and stability of the melt at the base of the lower mantle. Earth Planet. Sci. Lett. 193, 69–75.
Park, S.Y., Lee, S.K., 2012. Structure and disorder in basaltic glasses and melts: insights from high-resolution solid-state NMR study of glasses in diopside–Ca-tschermakite join and diopside–anorthite eutectic composition. Geochim. Cosmochim. Acta 80, 125–142.
Pei, F., Xu, W., Wang, Q., Wang, D., Lin, J., 2004. Mesozoic basalt and mineral chemistry of the mantle-derived xenocrysts in Feixian, Western Shandong, China: constraints on nature of Mesozoic lithospheric mantle. Geol. J. China Univ. 10, 88.
Revenaugh, J., Sipkin, S.A., 1994. Seismic evidence for silicate melt atop the 410 km mantle discontinuity. Nature 369 (6480), 474–476.
Rigden, S.M., Ahrens, T.J., Stolper, E.M., 1984. Densities of liquid silicates at high-pressures. Science 226, 1071–1074.
Rigden, S., Ahrens, T.J., Stolper, E., 1988. Shock compression of molten silicate: results for a model basaltic composition. J. Geophys. Res. 93 (B1), 367–382.
Sakamaki, T., Suzuki, A., Ohtani, E., 2006. Stability of hydrous melt at the base of the Earth's upper mantle. Nature 439, 192–194.
Sanchez-Valle, C., Bass, J.D., 2010. Elasticity and pressure-induced structural changes in vitreous $MgSiO_3$-enstatite to lower mantle pressures. Earth Planet. Sci. Lett. 295, 523–530.
Seifert, W.K., Moldowan, J.M., 1981. Paleoreconstruction by biological markers. Geochim. Cosmochim. Acta 45, 783–794.
Shim, S.-H., Catalli, K., 2009. Compositional dependence of structural transition pressures in amorphous phases with mantle-related compositions. Earth Planet. Sci. Lett. 283, 174–180.
Stolper, E.M., Ahrens, T.J., 1987. On the nature of pressure-induced coordination changes in silicate melts and glasses. Geophys. Res. Lett. 14, 1231–1233.
Stolper, E., Walker, D., Hager, B.H., Hays, J.F., 1981. Melt segregation from partially molten source regions: the importance of melt density and source region size. J. Geophys. Res., Solid Earth (1978–2012) 86, 6261–6271.
Suzuki, A., Ohtani, E., 2003. Density of peridotite melts at high pressure. Phys. Chem. Miner. 30, 449–456.
Suzuki, A., Ohtani, E., Kato, T., 1995. Flotation of diamond in mantle melt at high pressure. Science 269, 216–218.
Suzuki, A., Ohtani, E., Kato, T., 1998. Density and thermal expansion of a peridotite melt at high pressure. Phys. Earth Planet. Inter. 107, 53–61.
Tammann, G., Jenckel, E., 1929. Die Zunahme der Dichte von Gläsern nach Erstarrung unter erhöhtem Druck und die Wiederkehr der natürlichen Dichte durch Temperatursteigerung. Z. Anorg. Allg. Chem. 184, 416–420.
Tkachev, S., Manghnani, M., Williams, Q., 2005. In situ Brillouin spectroscopy of a pressure-induced apparent second-order transition in a silicate glass. Phys. Rev. Lett. 95, 057402.
Whitfield, C.H., Brody, E.M., Bassett, W.A., 1976. Elastic moduli of NaCl by Brillouin scattering at high pressure in a diamond anvil cell. Rev. Sci. Instrum. 47, 942–947.
Whittington, A.G., Richet, P., Polian, A., 2012. Water and the compressibility of silicate glasses: a Brillouin spectroscopic study. Am. Mineral. 97, 455–467.
Xie, H.-S., Zhang, Y.-M., Xu, H.-G., 1993. A new method of measurement for elastic wave velocities in minerals and rocks at high temperature and high pressure and its significance. Sci. China, Ser. B, Chem. Life Sci. Earth Sci. 36, 1276–1280.
Yan, Z.-T., 2000. An approximate relation between cubical thermal expansion coefficient of solids and pressure. Chin. J. High Press. Phys. 14, 4.
Yarger, J., Smith, K., Nieman, R., Diefenbacher, J., Wolf, G., Poe, B., McMillan, P., 1995. Al coordination changes in high-pressure aluminosilicate liquids. Science 270, 1964–1967.
Yoshino, T., Manthilake, G., Matsuzaki, T., Katsura, T., 2008. Dry mantle transition zone inferred from the conductivity of wadsleyite and ringwoodite. Nature 451, 326–329.